Surface & Coatings Technology 206 (2011) 348–353

Contents lists available at ScienceDirect

Surface & Coatings Technology

journal homepage: www.elsevier.com/locate/surfcoat

Electroless Ni-P plating on Mg-10Gd-4.8Y-0.6Zr magnesium alloy with a new pretreatment process

Jing Jin, Chuming Liu *, Shengli Fu, Yanrui Gao, Xin Shu

School of Materials Science and Engineering, Central South University, Changsha 410083, China

ARTICLE INFO

Article history:
Received 13 December 2010
Accepted in revised form 11 July 2011
Available online 20 July 2011

Keywords:
Mg-10Gd-4.8Y-0.6Zr magnesium alloy
New pre-treatment process
Electroless nickel plating
Corrosion resistance

ABSTRACT

A new pretreatment process for electroless Ni-P plating on Mg-10Gd-4.8Y-0.6Zr was investigated in this paper. The morphology, component, chemical composition and structure of the pretreatment layers and Ni-P coating were analyzed by scanning electronic microscopy, energy dispersive spectroscopy and X-ray diffraction spectroscopy. The structure of Ni-P coating was also detected by transmission electron microscopy (TEM). Potentiodynamic polarization analysis and salt spray test were used to test the corrosion resistance of the Ni-P coating. Experimental results indicate that: metal Cr generated in the new pretreatment process, which provided active points for later zinc immersion process, was beneficial to nickel deposition. The subsequent Ni-P coating was amorphous, in which the content of P was 9.43 wt.%. It was uniform and its thickness reached about 50 μm at 2 h deposition. Compared to Mg-10Gd-4.8Y-0.6Zr alloy substrate, the corrosion potential of the coated alloy shifted by 1090 mV positively and the corrosion current density decreased one order of magnitude in 3.5 wt.% NaCl solution. The salt spray test time of Ni-P coating was 210 h. All of these results suggest that the electroless nickel plating procedure researched in this paper is suitable for Mg-10Gd-4.8Y-0.6Zr alloy.

1. Introduction

Mg-Gd-Y-Zr magnesium alloys are widely investigated due to their excellent mechanical properties. They exhibit higher specific strength at both room and elevated temperatures and better creep resistance than conventional Al and Mg alloys, including WE54, whose high temperature strength is the top of existing commercial magnesium alloys [1–6]. However, the application of Mg-RE magnesium alloys has been limited due to their poor corrosion and wear resistance.

Electroless nickel plating is an effective method to increase the corrosion and wear resistance of magnesium alloys. Electroless nickel coatings are widely studied and used due to their special advantages, such as uniform deposition, good corrosion and wear resistance, good electrical and thermal conductivity, and good solder ability [7]. Many investigations related to electroless nickel plating on magnesium alloys have been reported. For example, Hui Zhao et.al [8] studied Ni-P coating formed on AZ31 magnesium alloys via electroless plating and organic coatings. N.El Mahallawy et.al [9] reported that electroless nickel plating on AZ31B, AE42 and ZRE1 wrought magnesium alloys with a zinc immersion pre-treatment. Yanrui Gao et.al [10] developed an appropriate and simplified process based on ZM6 alloy, the process flow was as follows: degrease → acid pickling → zinc immersion → nickel plating. W. X. Zhang et.al [11] investigated that a phosphate–manganese conversion film was proposed as the pretreatment layer between Ni-P coating and AZ91D alloy substrate. Hua Zhang et.al [12] explored the direct electroless Ni-P plating on Mg-10Li-1Zn alloy. However, there was few literature available related to coat Mg-Gd-Y-Zr alloys by electroless nickel plating.

Electroless nickel plating on magnesium alloys is faced with many challenges and the most difficult part of it is developing an appropriate pretreatment process. The existing pretreatment processes are not available for Mg-Gd-Y-Zr alloy, because compared to the commercial magnesium alloys, such as AZ91, AZ31, Mg-Gd-Y-Zr alloy contain heavy rare earth elements, which improve the tendency of magnesium to passivation [13,14]. In the present study, the authors explored a suitable electroless nickel plating procedure for Mg-Gd-Y-Zr magnesium alloy. The structure, morphology and corrosion resistance of the Ni-P coating were also studied.

2. Experimental

The experimental material used for this investigation is as-extruded Mg-10Gd-4.8Y-0.6Zr (wt.%) magnesium alloy with T5 treatment. Samples with a size of 15 mm × 10 mm × 4 mm were cut and abraded with No.1000 SiC paper. The electroless plating technique followed the procedure given in Table 1. All solutions used were freshly prepared from analytical grade reagents and deionized water. The samples were totally rinsed with distilled water after each step.

The morphologies and elemental composition of the pretreatment layers and the nickel coating were inspected respectively on Sirion

* Corresponding author: Tel: +86 731 8887 7502; fax: +86 731 8887 7502.
E-mail address: cmLiu@mail.csu.edu.cn (C. Liu).

0257-8972/$ – see front matter © 2011 Elsevier B.V. All rights reserved.
doi:10.1016/j.surfcoat.2011.07.023

Table 1
Compositions of bath and operating conditions of each process for nickel plating.

Process	Compositions	Operating conditions	
		Temperature	Time
Activation	$Cr_2(C_2O_4)_3$	Room temperature	30 s
Acid pickling	HNO_3	Room temperature	90–150 s
	CrO_3		
Post-activation	$Cr_2(C_2O_4)_3$	Room temperature	5–10 s
Zinc immersion	ZnO	82–86 °C	1 min
	HEDP		
	$C_2H_8N_2$ (ethylenediamine)		
	H_3PO_4		
Nickel plating	$NiCO_3 \cdot 2Ni(OH)_2 \cdot 4H_2O$	82–86 °C	2 h
	$NaH_2PO_2 \cdot H_2O$		
	HF		
	$C_3H_6O_3$ (lactic acid)		
	Brightener		

200 field emission scanning electron microscopy (SEM) with energy dispersive spectroscopy (EDS) system.

The structure of the pretreatment layers and nickel coating was measured using Rigaku D/Max 2500 X-ray diffraction (XRD) with Cu target. The XRD patterns were analyzed with MDI Jade5.0 software. The structure of the nickel coating was also detected by Tecnai G220 transmission electron microscope (TEM).

The corrosion resistance was evaluated by electrochemical tests and salt spray test. The electrochemical tests were carried out on electrochemical workstation using a classical three-electrode cell with platinum as counter electrode, saturated calomel electrode (SCE) as reference electrode, the substrate and Ni-P coating as working electrode. The potentiodynamic polarization was measured at a scan rate of 1 mV s^{-1}. The salt spray test was conducted according to ASTM B117 standard (5 wt.% NaCl spray,35 °C).

3. Results and discussion

3.1. The microstructure of the alloys

The optical and SEM micrograph of an as-extruded Mg-10Gd-4.8Y-0.6Zr alloy in T5 condition and EDS spectra of the phases are given in Fig. 1. Fig. 1a shows that the average grain size is about 30 μm. Fig. 1b (magnified in the top right corner) shows that the microstructure of the as-extruded alloy is composed of magnesium matrix, quadrate-like particle phases and round-like particle phases. Fig. 1c shows the EDS spectra of the quadrate-like particle phases. It exhibits the molar ratio between Mg and (GdY) approximately is 5:1, so the quadrate-like particle phases are $Mg_{24}(GdY)_5$. Fig. 1d shows the EDS spectra of the round-like particle phases. It proves that the round-like particle phases are Zr-rich cores. The microstructure of the as-extruded alloy in T5 condition is mainly composed of α-Mg, $Mg_{24}(GdY)_5$ and a little of Zr-rich cores[15,16]. The $Mg_{24}(GdY)_5$ phase mainly acts as galvanic cathode to accelerate the corrosion of magnesium matrix because of its higher potential. Obviously, galvanic interactions between the microstructure constituents have significant influence on the initial plating behavior.

3.2. Pre-treatment process

In this study, four pre-treatment processes shown in Table 1 were performed before electroless plating on Mg-10Gd-4.8Y-0.6Zr alloy. Fig. 2 shows the morphology of the specimen surface after different steps of pretreatment process. EDS results for element composition (wt.%) of the specimen surface are listed in Table 2. EDS results for element composition (wt.%) of the white particles in Fig. 2a, c, respectively, are listed in Table 3. The XRD patterns of the pre-treatment layers are shown in Fig. 3.

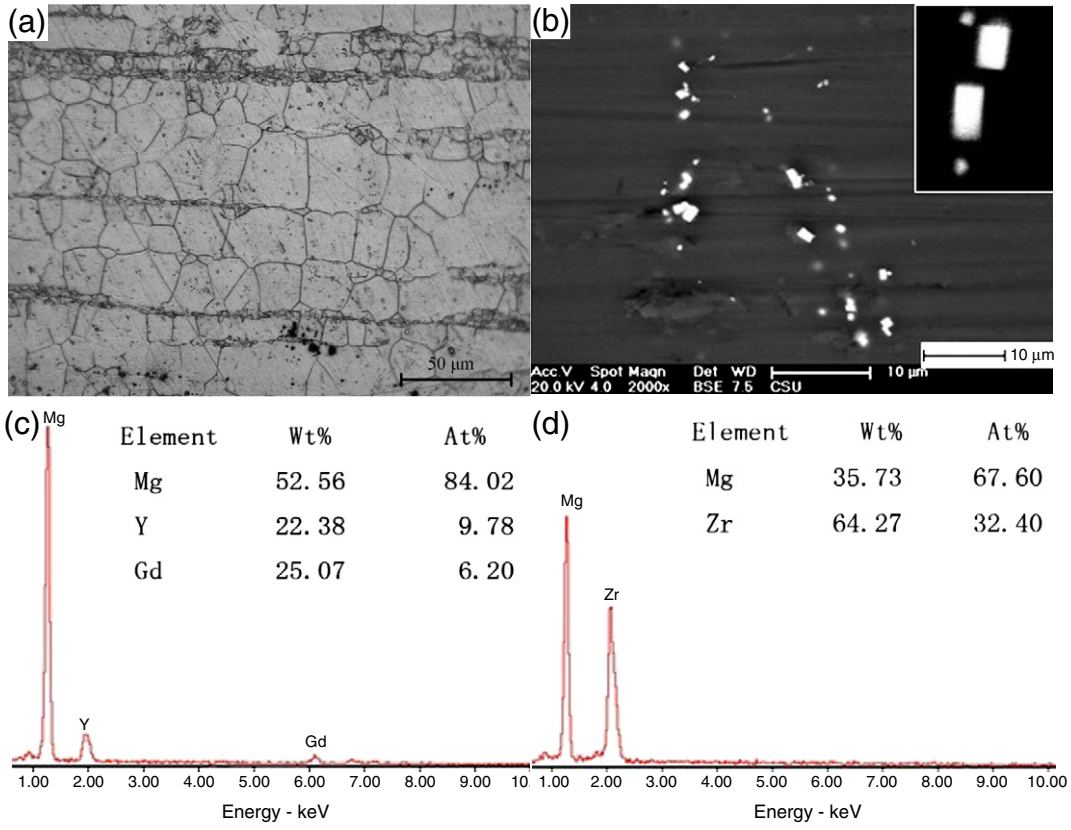

Element	Wt%	At%
Mg	52.56	84.02
Y	22.38	9.78
Gd	25.07	6.20

Fig. 1. Microstructure of as-extruded Mg-10Gd-4.8Y-0.6Zr alloy in T5 condition: (a) Optical image;(b) SEM image;(c) EDS spectra of the quadrate-like particle;(d) EDS spectra of the round-like particle.

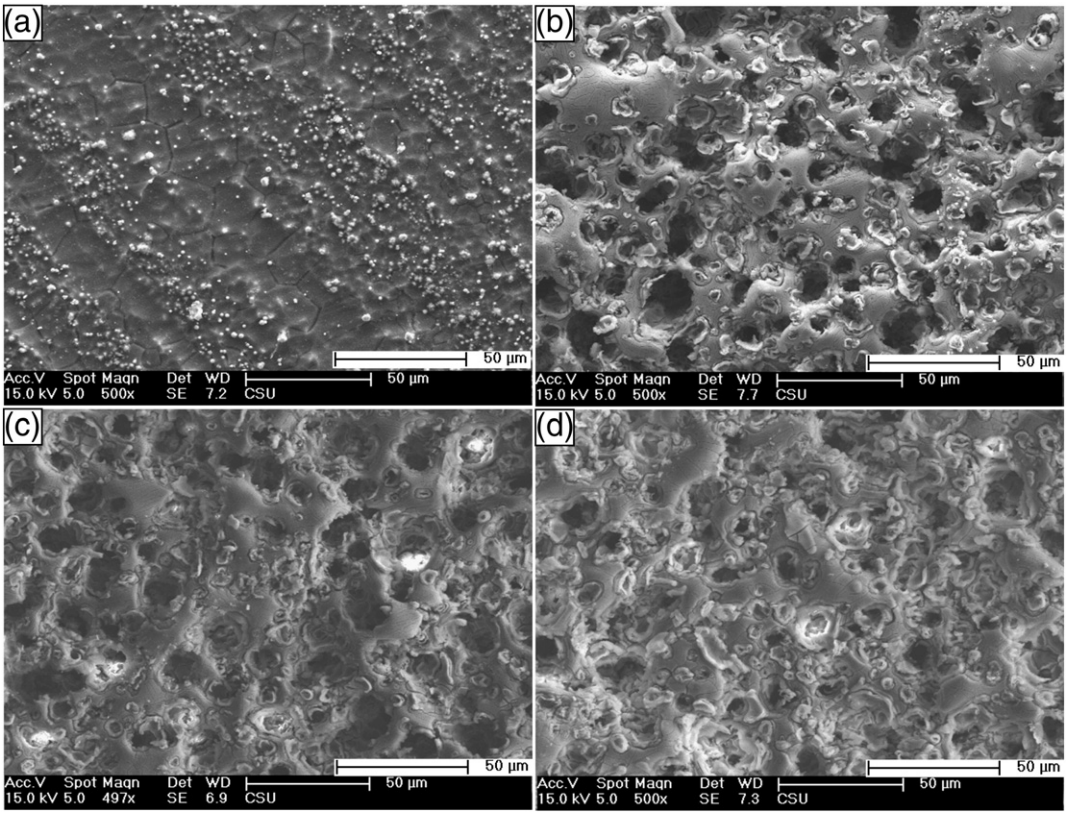

Fig. 2. SEM micrograph of the specimen surface after (a) activation; (b) acid pickling; (c) post-activation; (d) zinc immersion.

Activation was used to remove oxide and hydroxide film. After activation, there were plenty of white particles on the surface of the Mg substrate (Fig. 2a). The corresponding EDS result in Table 3 shows that the white particles mainly consisted of Cr, Mg, O elements, the percentage of Cr was up to 80.37 wt.%. Also the XRD pattern of the activation layer (Fig. 3b) shows that there were new metal Cr and MgO peaks produced, and the Mg peaks became weaker by comparison with the Mg substrate (Fig. 3a). It is believed that, MgO came from the oxidation reaction on the surface of the substrate, associated with the decrease of the acid concentration. The metal Cr was produced by the electrochemical reaction for activation:

$$\alpha - \text{Mg acted as local anode: } Mg \rightarrow Mg^{2+} + 2e \quad (1)$$

$$Mg_{24}(GdY)_5 \text{ acted as local cathode: } Cr^{3+} + 3e \rightarrow Cr \quad (2)$$

Table 2
Element composition (wt.%) of the specimen surface.

Samples	Mg	O	Cr	Zn
After activation	42.04	35.59	22.37	
After acid pickling	37.22	27.29	35.49	
After post-activation	33.76	27.09	39.14	
After zinc immersion	20.59	27.19	35.24	16.98

Table 3
Element composition (wt.%) of the white particles in Fig. 2a, c, respectively.

Samples	Mg	O	Cr
White-particles in Fig. 2a	1.81	17.82	80.37
White-particles in Fig. 2c	4.11	4.92	90.97

This indicates that the white particles were mainly metal Cr, deposited on the surface of the second phase to protect it from passivating in acid pickling solution and provided many active points for later zinc immersion process, which was beneficial to nickel deposition. However, the conventional electroless nickel plating procedures, such as direct electroless nickel plating procedure, did not activate before acid pickling, which would cause the heavy rare earth passivated in acid pickling solution and could not be activated by hydrogen fluoride acid. Finally, they created uneven or incomplete Ni-P coating.

Fig. 2b shows that the surface of the sample became rough after acid pickling, which could improve the adhesion of the Ni-P coatings and make the surface more chemically active [17]. Gao et al. [10]

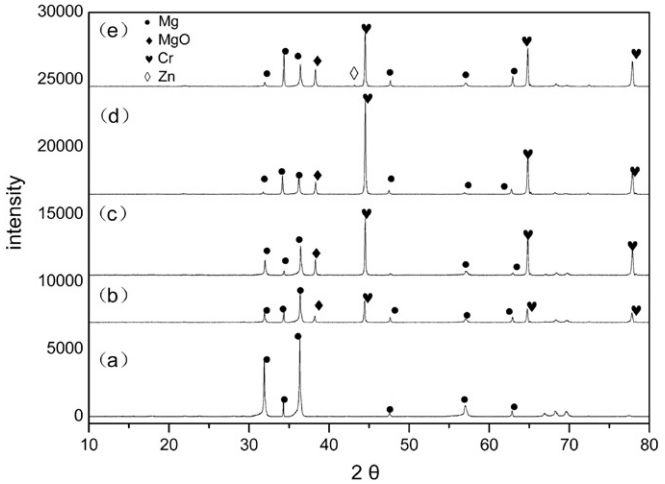

Fig. 3. The XRD patterns of Mg-10Gd-4.8Y-0.6Zr alloy (a) the substrate; (b) after activation; (c) after acid pickling; (d) after post-activation and (e) after zinc immersion.

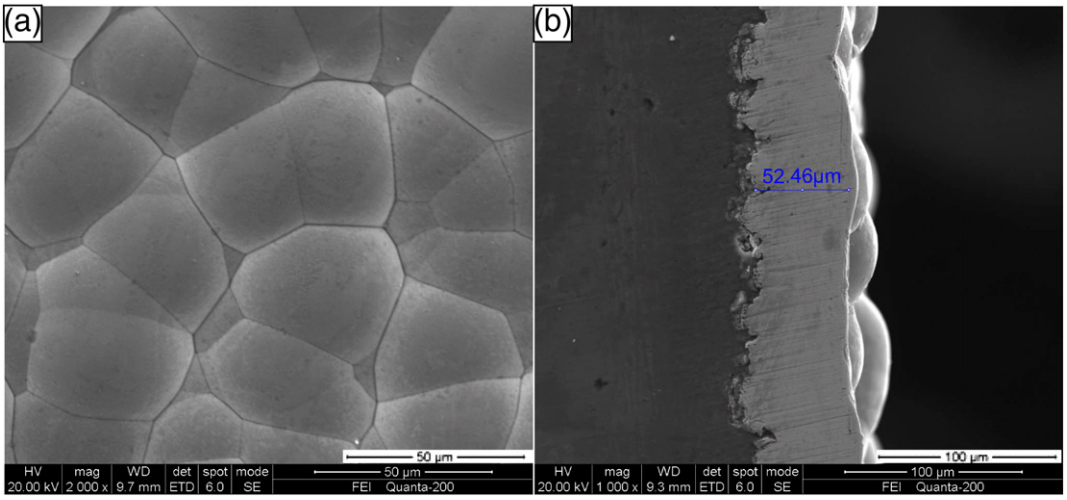

Fig. 4. SEM images of the electroless Ni-P coating after 2 h (a) surface morphology; (b) the corresponding cross-section morphology.

researched that acid pickling layer is composed of the compounds of $MgCrO_4$ and CrOOH, which could protect the Mg substrate from further corrosion. However, the two compounds could not be detected by X-ray diffraction spectroscopy (XRD) (Fig. 3c), because they were unspecific modality compounds. Fig. 3(c) also shows that the Mg peaks became much weaker. It can be explained by corroding the Mg substrate in the acid pickling solution.

Post-activation could remove the surplus acid pickling solution. Compared to Fig. 2b, it can be found that the white particles increased after post-activation (Fig. 2c). The corresponding EDS result in Table 3 shows that the white particles mainly consisted of Cr, Mg, O elements, the percentage of Cr was up to 90.97 wt.%. By the comparison of Fig. 3b–e, it can be concluded that the metal Cr content is the highest after post-activation, which is consistent with the EDS results shown in Table 2. These results indicate that the weaker protection film produced in the acid pickling treatment was destroyed, and then the exposed Mg substrate reacted with the post-activation solution following Eqs. (1) and (2) to get metal Cr. The metal Cr could provide much more active points for later zinc immersion treatment. It served as a metal conductor in the zinc immersion electrochemical reaction process, which can make more Mg substrate react with Zn^{2+}.

The final zinc immersion treatment (Fig. 2d) is an indispensable step to create many active points for later electroless nickel plating process, accompanying with the hydrogen evolution and Mg dissolution. EDS results in Table 2 show that elements Mg, Cr, Zn and O are contained on the surface of the specimen. The corresponding XRD patterns of zinc immersion layer (Fig. 3e) show that a new Zn peaks produced, but the metal Cr peaks decreased. It could be explained by the electrochemical reaction in the zinc immersion treatment:

$$\text{Mg served as local anode: } Mg \rightarrow Mg^{2+} + 2e \tag{3}$$

$$\text{Metal Cr acted as a local cathode: } Zn^{2+} + 2e \rightarrow Zn \tag{4}$$

The metal Cr was covered by the deposited Zn, which leaded to the decrease of the metal Cr peaks. Metal Zn has no catalytic property as Fe, Co, and Ni, and the reducibility of nickel ions by hypophosphite cannot be carried out. However, the metal nickel can be produced by replacement reaction in initial nickel deposition, such as $Zn + Ni^{2+} \rightarrow Zn^{2+} + Ni$. Then the precursor nickel particles exhibit catalytic property, and they can act as nuclei centers to form Ni-P coatings in terms of autocatalytic reaction. The overall reaction of electroless Ni-P deposition in acidic hypophosphite bath can be broadly expressed as [18]:

$$\text{Anodic reaction: } H_2PO_2^- + H_2O \rightarrow H_2PO_3^- + 2H^+ + 2e \tag{4}$$

$$\text{Cathodic reactions: } Ni^+ + 2e \rightarrow Ni \tag{5}$$

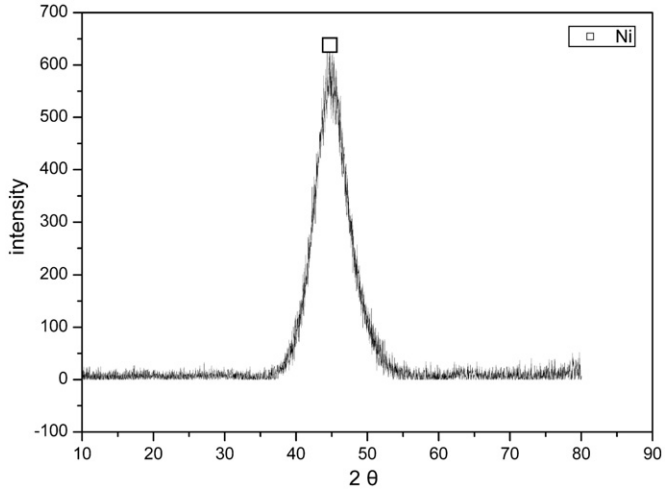

Fig. 5. The XRD patterns of the electroless Ni-P coating on Mg-10Gd-4.8Y-0.6Zr alloy.

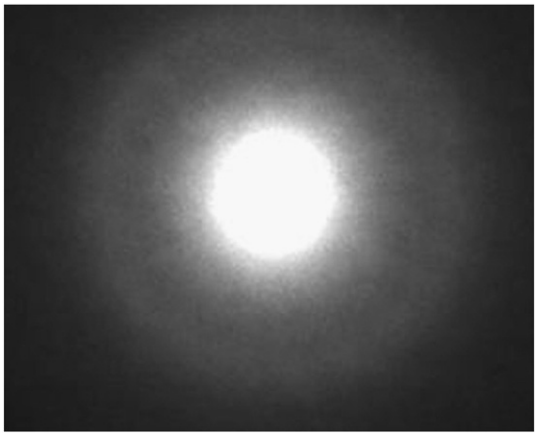

Fig. 6. The selected area diffraction pattern of the Ni-P coating on Mg-10Gd-4.8Y-0.6Zr alloy.

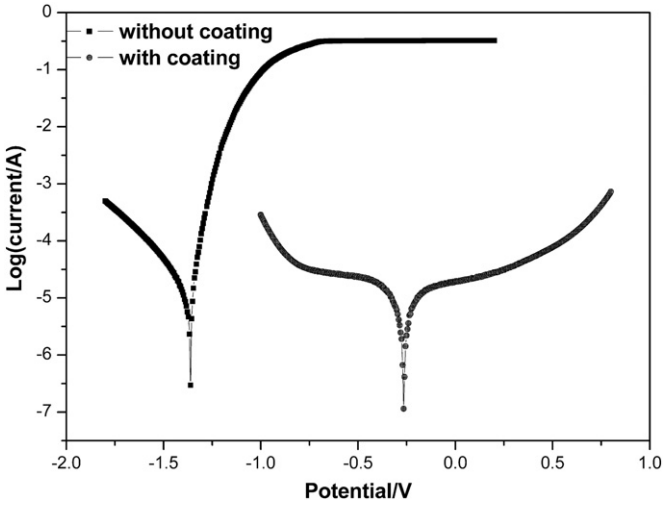

Fig. 7. Polarization curves of Mg-10Gd-4.8Y-0.6Zr alloy substrate and Ni-P coating in 3.5 wt.% NaCl solution.

Table 4
Corrosion potential and corrosion current density obtained from the polarization curves.

Sample	E_{corr}/V	$i_{corr}/(A \cdot cm^{-2})$
Mg-10Gd-4.8Y-0.6Zr alloy substrate	−1.351	8.718×10^{-6}
Ni-P coating	−0.261	4.144×10^{-7}

$$2H^{+} + 2e \rightarrow H_2 \quad (6)$$

3.3. The morphology, structure and corrosion resistance of Ni-P coating

3.3.1. The morphology of Ni-P coating

The morphology of the electroless Ni-P coating on the Mg-10Gd-4.8Y-0.6Zr alloy at a plating time for 2 h, detected by SEM is shown in Fig. 4.

Fig. 4(a) indicates that the electroless nickel coating is composed of compact fine nodules with uniform size. The surface of Ni-P coating was compact, uniform and shows the typical spherical nodular structure. The present EDS result indicates that P content of the coating was about 9.4 wt.%. It shows that the Ni-P coating with high phosphorus content could improve corrosion resistance as compared to low- and medium-phosphorus containing coatings [19]. Fig. 4(b) seems that there is no obvious interfacial boundary between the coating and the substrate, which exhibits excellent adhesion. The thickness of the coating was about 50 μm. It can be explained by that the acid pickling pretreatment makes the surface of the magnesium alloy become rough, which provides corroded surface to act as sites for mechanical interlocking to improve adhesion and deposition rate [20].

3.3.2. Analysis of the Ni-P coating

Fig. 5 shows the diffraction pattern of the Ni-P coating. There is only a single very broad peak at 2θ–45°, which indicates that the structure of the Ni-P coating is amorphous. Fig. 6 shows the selected area diffraction pattern of the Ni-P coating. It exhibits a diffuse ring pattern which is typical of an amorphous structure. There is no grain boundary, dislocation and composition segregation in the amorphous Ni-P coating and the homogeneous microstructure on the surface of the Ni-P coating is hardly to produce a galvanic coupling. Therefore, a conclusion can be drawn that the amorphous structure can improve the corrosion resistance of the Ni-P coating, which has been proved by the results of the electrochemical tests.

3.3.3. Corrosion resistance of Ni-P coating

The results of the electrochemical tests are shown in Fig. 7. It presents the potentiodynamic curves of the bare and Ni-P coated Mg-10Gd-4.8Y-0.6Zr alloy in 3.5 wt.% NaCl solution at room temperature. Fitting results are given in Table 4. It can be obviously seen that the coating exhibited a less negative corrosion potential(E_{corr}) and a lower corrosion current(I_{corr}) than the bare alloy; the corrosion potential of samples with coating shifted by 1090 mV positively and the corrosion current density decreased by one order of magnitude compared to the bare alloy. It implies that anodic dissolution reaction of the Ni-P coating was restrained, which effectively decreased the corrosion sensibility of the coated sample in NaCl solution. These demonstrate that the electroless Ni-P coating provides a good protection for Mg-10Gd-4.8Y-0.6Zr bare alloy.

Fig. 8 shows the appearance of the samples after salt spray test. The Ni-P coating survived in the salt spray test up for 210 h (Fig. 8a), while it was only 6 h for the uncoated Mg-10Gd-4.8Y-0.6Zr alloy (Fig. 8b). This indicates an excellent anti-corrosion performance of the as-plated Ni-P coating.

4. Conclusions

The new pretreatment process has been adapted to successfully plate a uniform and compact Ni-P coating on Mg-10Gd-4.8Y-0.6Zr alloy. The main results can be summarized as follows:

(1) There was metal Cr produced in the new pretreatment process. It could provide many active points for later zinc immersion process, which was beneficial to nickel deposition.
(2) The Ni-P coating was amorphous, compact with good adhesion, and the thickness reached approximately 50 μm at a plating time of 2 h. The P content of the coating was 9.43 wt.%.

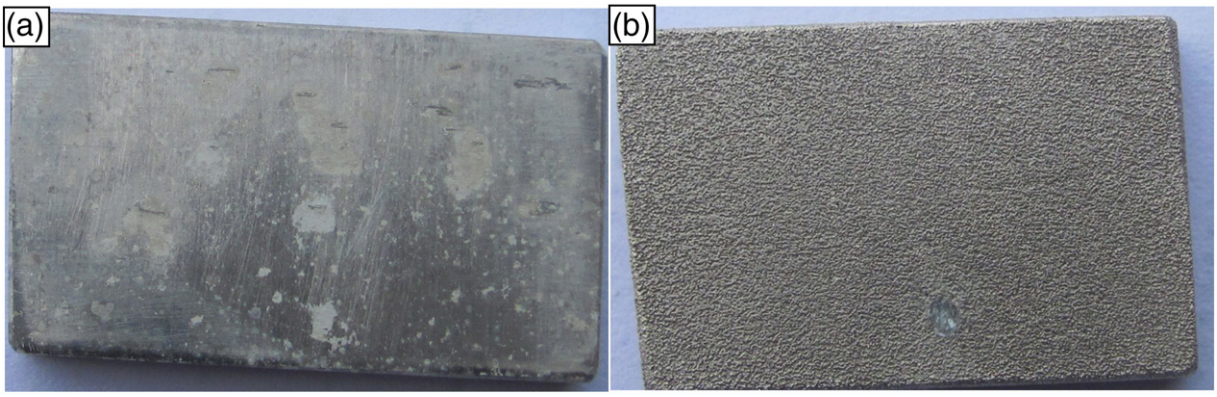

Fig. 8. Photos for appearance of samples after salt spray test (a) appearance of the substrate after 6 h test; (b) appearance of Ni-P coating after 210 h test.

(3) Ni-P coating can provide a good corrosion protection for the Mg-10 Gd-4.8Y-0.6Zr alloy. Its corrosion potential shifted by 1090 mV positively and the corrosion current density decreased by one order of magnitude. The salt spray test time of Ni-P coating was 210 h.

Acknowledgments

This work was supported partly by the Natural Science Foundation of China (51074186) and the Open-End Fund for the valuable and Precision Instruments of Central South University. The authors would like to thank Professor Chuming Liu and Daoyun Ding for providing writing assistance to the article, and the helpful comments given by the anonymous reviewers.

References

[1] Y. Liu, G.Y. Yuan, C. Lu, W.J. Ding, Scripta Mater. 55 (2006) 919.
[2] S.M. He, X.Q. Zeng, L.M. Peng, J. Alloys Compd. 427 (2007) 316.
[3] S.M. He, X.Q. Zeng, L.M. Peng, J. Alloys Compd. 421 (1–2) (2006) 309.
[4] B. Smola, I. Stulíková, F. von Buch, B.L. Mordike, Mater. Sci. Eng. A 324 (2002) 113.
[5] I. Anthony, S. Kamado, Y. Kojima, Mater. Trans. 42 (2001) 1206.
[6] I. Anthony, S. Kamado, Y. Kojima, Mater. Trans. 42 (2001) 1212.
[7] S. Sun, J.G. Liu, C.W. Yan, F.H. Wang, Appl. Surf. Sci. 254 (2008) 5016.
[8] H. Zhao, Z.H. Huang, J.Z. Cui, Surf. Coat. Technol. 202 (2007) 133.
[9] N.El. Mahallawy, A. Bakkar, M. Shoeib, H. Palkowski, V. Neubert, Surf. Coat. Technol. 202 (2008) 5151.
[10] Y.R. Gao, C.M. Liu, S.L. Fu, J. Jin, X. Shu, Y.H. Gao, Surf. Coat. Technol. 204 (2010) 3629.
[11] W.X. Zhang, J.G. He, Z.H. Jiang, Q. Jiang, J.S. Lian, Surf. Coat. Technol. 201 (2007) 4954.
[12] H. Zhang, S.L. Wang, G.C. Yao, Z.S. Hua, J. Alloys Compd. 474 (2009) 306.
[13] F. Zucchi, V. Grassi, A. Frignani, C. Monticelli, G. Trabanelli, J. Appl. Electrochem. 36 (2006) 195.
[14] I. Nakatsugawa, S. Kamado, Y. Kojima, R. Ninomiya, K. Kubota, Corros. Rev. 16 (1998) 139.
[15] X. Zhang, L. Li, Y. Deng, N. Zhou, J. Alloys Compd. 481 (2009) 296.
[16] Y.C. Guo, J.P. Li, J.S. Li, Z. Yang, J. Zhao, F. Xia, M.X. Liang, J. Alloys Compd. 450 (2008) 446.
[17] Z.M. Liu, W. Gao, Surf. Coat. Technol. 200 (2006) 3553.
[18] H.W. Huo, Y. Li, F.H. Wang, Corros. Sci. 46 (2004) 1467.
[19] B. Lonyuk, I. Apachitei, J. Duszczyk, Scripta Mater. 57 (2007) 783.
[20] H.C. Bi, Y.H. Wei, L.F. Hou, C.Y. Yu, L.Q. Hu, B.S. Xu, Rare Met. Mater. Eng. 10 (2006) 1661.